Localized compliance of small airways in excised rat lungs using microfocal X-ray computed tomography

Toshihiro Sera, Hideki Fujioka, Hideo Yokota, Akitake Makinouchi, Ryutaro Himeno, Robert C. Schroter and Kazuo Tanishita

J Appl Physiol 96:1665-1673, 2004. First published 6 February 2004;
doi:10.1152/japplphysiol.00624.2003

J Appl Physiol 96: 1665–1673, 2004.
First published February 6, 2004; 10.1152/japplphysiol.00624.2003.

Localized compliance of small airways in excised rat lungs using microfocal X-ray computed tomography

Toshihiro Sera,[1,2] Hideki Fujioka,[3] Hideo Yokota,[4] Akitake Makinouchi,[5] Ryutaro Himeno,[4] Robert C. Schroter,[6] and Kazuo Tanishita[7]

[1]*Center for Life Science and Technology, School of Fundamental Science and Technology, and* [7]*Department of System Design Engineering, Keio University, Yokohama 223-8522;* [4]*Advanced Computing Center and* [5]*Integrated V-CAD System Research Program, Institute of Physical and Chemical Research (RIKEN), Wako, Saitama 351-0198; and* [2]*Life and Environmental Science Division, Japan Synchrotron Radiation Institute (SPring-8), Hyogo 679-5198, Japan;* [3]*Biomedical Engineering Department, The University of Michigan, Ann Arbor, Michigan 48109-2099; and* [6]*Department of Bioengineering, Imperial College London, London SW7 2AZ, United Kingdom*

Submitted 17 June 2003; accepted in final form 18 December 2003

Sera, Toshihiro, Hideki Fujioka, Hideo Yokota, Akitake Makinouchi, Ryutaro Himeno, Robert C. Schroter, and Kazuo Tanishita. Localized compliance of small airways in excised rat lungs using microfocal X-ray computed tomography. *J Appl Physiol* 96: 1665–1673, 2004. First published February 6, 2004; 10.1152/japplphysiol.00624.2003.—Airway compliance is a key factor in understanding lung mechanics and is used as a clinical diagnostic index. Understanding such mechanics in small airways physiologically and clinically is critical. We have determined the "morphometric change" and "localized compliance" of small airways under "near"-physiological conditions; namely, the airways were embedded in parenchyma without dehydration and fixation. Previously, we developed a two-step method to visualize small airways in detail by staining the lung tissue with a radiopaque solution and then visualizing the tissue with a cone-beam microfocal X-ray computed tomography system (Sera et al. *J Biomech* 36: 1587–1594, 2003). In this study, we used this technique to analyze changes in diameter and length of the same small airways (~150 μm ID) and then evaluated the localized compliance as a function of airway generation (*Z*). For smaller (<300-μm-diameter) airways, diameter was 36% larger at end-tidal inspiration and 89% larger at total lung capacity; length was 18% larger at end-tidal inspiration and 43% larger at total lung capacity than at functional residual capacity. Diameter, especially at smaller airways, did not behave linearly with $V^{1/3}$ (where V is volume). With increasing lung pressure, diameter changed dramatically at a particular pressure and length changed approximately linearly during inflation and deflation. Percentage of airway volume for smaller airways did not behave linearly with that of lung volume. Smaller airways were generally more compliant than larger airways with increasing *Z* and exhibited hysteresis in their diameter behavior. Airways at higher *Z* deformed at a lower pressure than those at lower *Z*. These results indicated that smaller airways did not behave homogeneously.

soft tissue; morphometry change; tissue elasticity; surface tension

TO EVALUATE RESPIRATORY FUNCTION in detail, not only the overall compliance, as given by the gradient ($\Delta V/\Delta P$, where V is volume and P is pressure) of the P-V curve, based on the relation between lung pressure and lung volume, but also the more localized compliance, based on microscopic regions of parenchyma and airways, needs to be determined. The overall P-V curve of the lung describes bulk compliance and hysteresis, which are dominated by tissue elasticity and surface tension. Respiratory diseases, however, occur most frequently at small airways (26), and the condition of small airways has important physiological and clinical implications. In many respiratory diseases, significant compliance abnormalities mainly occur in localized regions of bronchi and bronchioles, and thus, in addition to the overall compliance, the localized, or the microscopic, compliance of parenchyma and small bronchi or bronchioles based on small-scale observations must be identified.

Many studies have dealt with airway dynamics (7), surfactant transport (1, 31), and particle deposition (2) that occur in small airways. The concept of analyzing the microscopic compliance was introduced in the 1970s by Hughes et al. (8), Menkes et al. (15), and Sittipong and Hyatt (23). They insufflated tantalum powder into a lung as a contrast agent and then used bronchograms to analyze regional volume changes and changes in diameter and length of individual bronchial segments at various transmural pressures. However, those measurements were limited to large (>0.5-mm-diameter) bronchi.

Two principles have been used to analyze the mechanical properties of small airways. One approach is to visualize dehydrated and fixed preparations by using optical microscopy (10, 18). However, the preparation procedure significantly deforms the sample tissue, and it is extremely difficult to observe the morphometric changes of the same airways at various lung volumes. The other approach is to measure the mechanical properties of excised small airway segments in vitro (27). However, in situ, the intrapulmonary airways are surrounded by lung parenchyma, and the effective microscopic airway compliance is influenced by the surrounding support (Fig. 1). The larger intrapulmonary bronchi are surrounded by the peribronchial sheath (an invagination of the visceral pleura), which in turn is connected to the alveolar parenchyma. At some anatomically unspecified distance along the peripheral bronchial tree, the bronchi penetrate the peribronchial sheath and become directly connected to the parenchyma. As a consequence, the surface pressure acting on the larger bronchi is the pressure within the peribronchial space, which may be lower (more negative) than the effective pressure exerted by the parenchyma directly, as is the case for the smallest airways;

Address for reprint requests and other correspondence: T. Sera, Life and Environmental Science Div., Japan Synchrotron Radiation Research Institute, SPring-8, 1-1-1 Kouto, Mikazuki, Sayo, Hyogo 679-5198, Japan (E-mail: sera@spring8.or.jp).

The costs of publication of this article were defrayed in part by the payment of page charges. The article must therefore be hereby marked "*advertisement*" in accordance with 18 U.S.C. Section 1734 solely to indicate this fact.

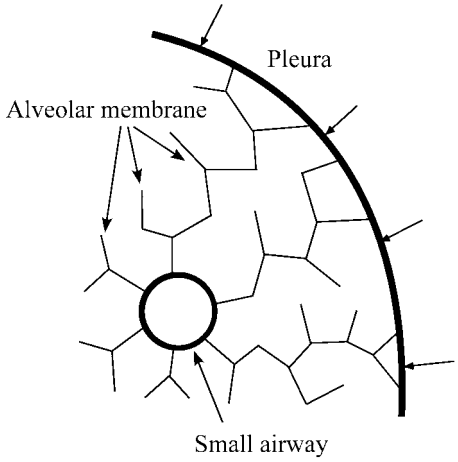

Fig. 1. Schematic model of a small airway in lung parenchyma.

this difference in pressure, however, may not be large unless inhomogeneous conditions, such as forced expiration, are undertaken. Hyatt and Flath (9) and Takishima et al. (25) measured diameter and length behavior of large (>1-mm-diameter) airways and reported that intact airways are stiffer than excised airways. No accurate measurements have been reported for small intact airways.

In this study, we hypothesize that small airways were also stiffened in parenchyma, and their diameter-volume relation will not follow that of the surrounding parenchyma. The length-volume relation would be expected to follow the conventional proportionality to $V^{1/3}$ to reflect the overall need to maintain connectivity and be space filling.

We determined diameters, lengths, and "localized compliance" of small airways to establish their mechanical properties. This localized compliance reflects the compliance of restricted regions under "near"-physiological conditions, in which small airways are embedded in lung parenchyma without dehydration and fixation. The measurements can be used potentially as a physiological and a clinical index.

We previously developed the staining-and-CT (SCT) imaging method to visualize small airways in detail by staining the lung tissue with a radiopaque solution and then visualizing the tissue by using a cone-beam microfocal X-ray CT system (21). In the present study, we visualized the three-dimensional structure of small airways of an excised rat lung by using the SCT method, analyzed the diameter and length of the same small airways at various lung volumes by using a three-dimensional thinning (skeletonization) algorithm, and then evaluated the localized compliance in the airway generation (Z) from 8 to 16, where Z is the number of bifurcations from the trachea to the airway of interest as proposed by Weibel (30).

Our results show that not all airway generations deform in the same manner. During earlier and later steps of static P-V curves, small airways behaved similarly to large airways. However, the diameter of small airways did not behave linearly with $V^{1/3}$, and the percentage of airway volume for the small airways was not similar to that of lung volume. The diameter of the small airways changed dramatically at a specific lung pressure with increasing lung pressure, although the length changed linearly. The smaller airways exhibit hysteresis, especially in their diameter, and the localized compliance increases with Z. These results indicated that the small airways did not behave homogeneously.

MATERIALS AND METHODS

Animal preparation. All animals used in the experiments received humane care, and the experimental protocol was approved by the Committee of Laboratory Animals according to Keio University guidelines. The excised rat lungs were prepared as described previously (21). Sixteen male Wistar rats (300 ± 30 g) were anesthetized with pentobarbital sodium (50 mg/kg ip), and the inferior vena cava (IVC) was cannulated and perfused with a 0.9% saline solution for 5 min at a flow rate of 5–40 ml/min. The IVC was cannulated with the chest open, but during the whole procedure the lungs were kept inflated at functional residual capacity (FRC). After the saline solution was drained through the pulmonary veins, saline with 0.2 g/ml KCl solution was injected into the IVC to induce cardiac arrest. Diatrizoate sodium solution (0.8 g/ml; Sigma Chemical, St. Louis, MO) was then injected into the pulmonary arteries via the IVC cannula for 1 min at a flow rate of 5–40 ml/min. Complete staining of the lungs by the diatrizoate solution was ensured by exposure of the preparations to ambient air for 1 h. To prevent desiccation, we placed cotton moistened with a 0.9% saline solution on the lungs. Finally, the lungs were excised, while the volume was maintained at FRC; then the lungs were placed into a Plexiglas cylinder to prevent desiccation during the acquisition of micro-CT images (Fig. 2).

Measurements. The bulk static P-V curves of the lungs were determined by stepwise inflation of the lungs in 1-ml increments to total lung capacity (TLC) and deflation in 1-ml decrements to FRC. The pressure and volume of the stained excised lungs in the cylinder could be externally regulated. Pressure was measured by using a pressure transducer (model EPI-541-0.35B, Entran) that had been calibrated using a manometer. In this study, we injected radiopaque solution into the pulmonary arteries via the IVC to stain the lung tissue, while the chest was opened and the lungs were kept inflated at FRC. As a result of this procedure, we could not measure the volume at FRC accurately. However, in previous studies using body plethysmography, saline displacement, and a neon dilution method, rat FRC was 2.5–3.7 ml (11, 12, 24). Therefore, in this present study, we arbitrarily, but reasonably, defined the volume at FRC as 3 ml. The volume (TV) was defined as FRC + 2 ml, which approximated the anticipated tidal volume (7 ml/kg). TLC was defined as FRC + 8 ml, and pressure at TLC was 26.52 ± 2.25 cmH_2O. The lungs were inflated and deflated to various volumes using a 1-ml glass syringe at an accuracy of 0.02 ml, and micro-CT images (see *Imaging*) were obtained.

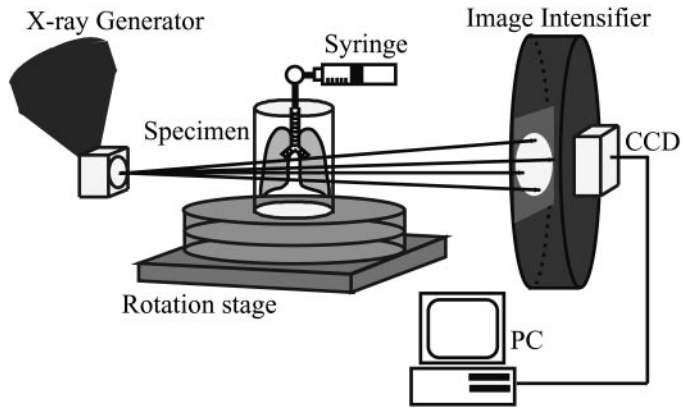

Fig. 2. Experimental apparatus of the micro-CT system consisting of a microfocal cone-beam X-ray source (spot size = 7 μm), an x-y-z-θ rotation stage, an image intensifier, and a 12-bit charge coupled device (CCD) camera. Excised rat lung in the Plexiglas cylinder was mounted on the rotation stage.

Imaging. The small airways were imaged using a microfocal X-ray CT system (model MCT-CB100MF, Hitachi Medical, Japan, Tokyo; Fig. 2). To reconstruct the CT images, a summed projection was acquired at 625 rotational positions. The resolution was 480 × 480 pixels, and 200 slice images per rotation were obtained. To visualize small airway networks, 1 cubic voxel was 16 μm, which meant that 1 square pixel was 16 × 16 μm and the space between each image was also 16 μm. All images of the excised rat lung over a 360° rotation were obtained in 2.5 min. Before taking CT images, we confirmed that the lung pressure was stable for 1 min at each lung volume. If there were air leaks during a sample rotation, the reconstructed CT images had some artifacts due to the high-resolution CT systems. To determine the diameter (D) and length (L) of an airway, the same branching networks were visualized for a volume between FRC and TLC during a stepwise inflation process in 2-ml increments and the deflation process in 2-ml decrements. The experimental time from the initial to the final measurement (including image reconstructions) was <2 h.

Analysis. To determine the morphometry of the small airways, we identified the cross sections of the small airways by using the threshold method (21) and then analyzed these cross sections by using the three-dimensional thinning algorithm of Toriwaki and Mori (28). This algorithm involves the Euclidean distance transformation and repeatedly checks the deletability of points in a sequence in which the Euclidean distance value is small and, finally, finds the skeletonized lines and the branching points of the airway network without changing the topology of the airways. However, this algorithm left "false" spurs, which we removed "manually" until the middle lines agreed with the input images.

The L and D of the airways were determined by approximating the airway as a cylinder network (21). The fractional increases in L and D (δ_L and δ_D, respectively), normalized by L and D at FRC (L_{FRC} and D_{FRC}, respectively), were calculated as follows

$$\delta_L = \frac{L' - L_{FRC}}{L_{FRC}}$$

$$\delta_D = \frac{D' - D_{FRC}}{D_{FRC}}$$

where L' and D' are expressed as L and D at each lung volume.

In this study, the localized compliances C_{TV} and C_{TLC} of the airways were evaluated at volumes defined by the volume infused (based on the volume infused by the syringe) to inflate the airways from FRC to TV and from FRC to TLC as follows

$$C_{TV} = \frac{(D_{TV}^2 \cdot L_{TV} - D_{FRC}^2 \cdot L_{FRC})}{\Delta P_{TV} \cdot D_{FRC}^2 \cdot L_{FRC}}$$

$$C_{TLC} = \frac{(D_{TLC}^2 \cdot L_{TLC} - D_{FRC}^2 \cdot L_{FRC})}{\Delta P_{TLC} \cdot D_{FRC}^2 \cdot L_{FRC}} \quad (1)$$

To determine Z, we macroscopically imaged the entire lung by using micro-CT (1 cubic voxel of 43 × 43 × 43 μm) and identified the generation of the airways manually.

Statistical analysis. The size changes and the localized compliance are presented as means ± SE as a function of Z (n = 7–17 per Z) and lung condition (volume and pressure; n = 18–45 per lung condition). The lungs used during the inflation measurement process were different from those used during the deflation process. Differences between inflation and deflation groups and between each lung condition were tested for significance by analysis of variance followed by Tukey-Kramer multiple comparisons. Differences in δ_D, δ_L, C_{TV}, and C_{TLC} as a function of Z were also assessed for significance by analysis of variance followed by Steel-Dwass multiple comparisons. $P < 0.05$ was considered to be statistically significant.

RESULTS

Rat lung tissue was stained by a radiopaque solution perfused into the pulmonary vessels, and thus the small airway lumina were easily distinguishable from lung tissue. Figure 3 shows a representative micro-CT image of the stained tissue. The pixel intensity of the lung tissue was much stronger than that of air spaces, and thus the regions of brightest intensity correspond to lung tissue and pulmonary vessels, as indicated in Fig. 3. The small airways and alveoli are visible as black regions.

The three-dimensional structure of the same branching networks at FRC and TLC was reconstructed on the basis of the tomographic images using an isosurface approach in the Visualization Toolkit, which is an open-source, object-oriented software system for three-dimensional computer graphics and imaging processing used by many researchers (Kitware, http://www.kitware.com/). Figure 4 shows the reconstructed three-dimensional structure. The branching networks expanded dramatically in three dimensions from FRC to TLC. D and L of each airway segment were increased at TLC compared with D and L at FRC, although δ_D was larger than δ_L.

Bronchial hysteresis. Figure 5 shows the overall P-V relation for whole lungs with the representative bronchial hysteresis illustrated at a given lung pressure (10 cmH_2O), and Fig. 6 shows the same at a given lung volume (TV); the P-V curves and CT images in Figs. 5 and 6 were obtained from the same lung. A 1-ml glass syringe was used to inject air in 2-ml increments into the lungs from FRC to TLC. When pressure was stabilized, it was measured, and further increments of air were injected. The entire stained excised rat lung exhibited lung hysteresis in the overall P-V curve (Figs. 5 and 6, *top*),

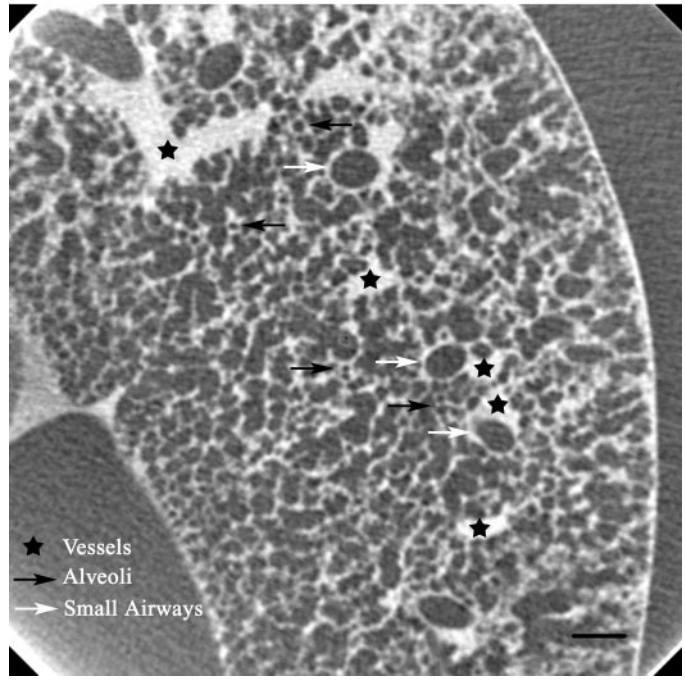

Fig. 3. Representative micro-CT image showing many small airways and alveoli at functional residual capacity (FRC; 1 square pixel = 16 × 16 μm). Diatrizoate sodium stained the lung tissue; therefore, airway lumina with air had weaker intensity. Arrows, airways [small airways (white arrows) and alveoli (black arrows)]; ★, vessels. Scale bar, 500 μm.

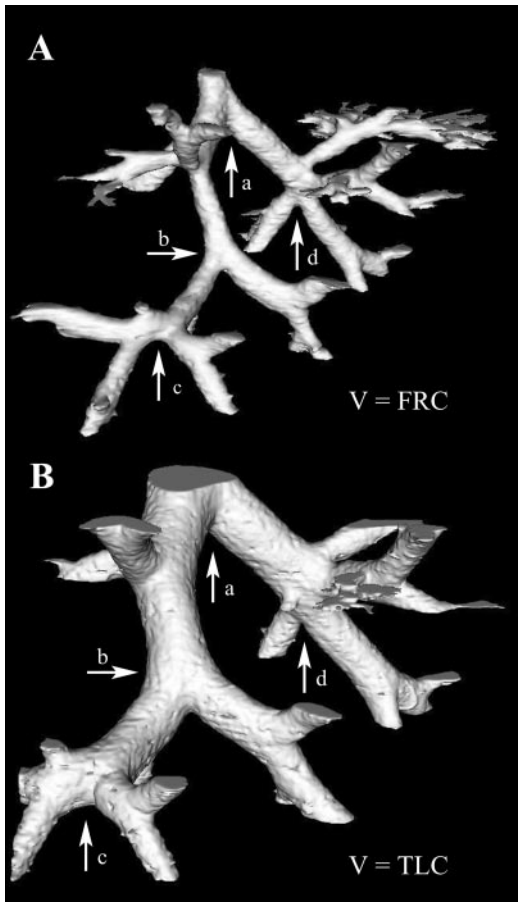

Fig. 4. Three-dimensional structures of the same branching network at FRC (*A*) and total lung capacity (TLC, *B*). Airway diameter range at FRC was 300–170 μm. Airway generation (*Z*) range was 10–16. Arrows (*a–d*) indicate the same dividers in *A* and *B*. V, volume.

and the bronchial *D* (arrows in Figs. 5 and 6, *bottom*) was larger during deflation than during inflation at the same pressure and the same volume. At 10 cmH_2O pressure, *D* was 1.28–1.44 times larger during deflation (Fig. 5*D*) than during inflation (Fig. 5*B*), and at TV *D* was 1.21–1.35 times larger during deflation (Fig. 6*D*) than during inflation (Fig. 6*B*). These results indicated hysteresis of localized alveolar regions in the vicinity of the small airways.

Bronchial diameter. Figure 7 shows the average δ_D at TV and TLC during inflation as a function of *Z*. δ_D increased with *Z*, and δ_D of TV and δ_D of TLC were statistically larger at $Z = 16$ than at $Z = 8$ ($P < 0.01$), and δ_D of TLC was significantly larger than δ_D of TV at $Z = 11$–16 ($P < 0.05$). These results are consistent with those reported previously (23).

Figure 8 shows representative changes in the cross section of a small airway during inflation and deflation. During inflation, *D* remained relatively constant between FRC and FRC + 4 ml and started to increase between FRC + 4 ml and FRC + 6 ml. In contrast, during deflation, *D* remained approximately constant between TLC and TLC − 6 ml and started to decrease at TLC − 6 ml, indicating that the local cross-sectional change shows typical hysteresis in the overall lung P-V curve.

Figure 9 shows the percentage of average *D* for the larger (>300-μm-diameter) and smaller (<300-μm-diameter) airways as a function of the percentage of $V^{1/3}$. During the inflation process, the percentage of *D* for smaller airways was significantly larger at $(TV + 4\ ml)^{1/3}$ than at $(TV + 2\ ml)^{1/3}$ ($P < 0.001$). Also, the percentage of *D* for smaller airways at $TV^{1/3}$ and $(TV + 2\ ml)^{1/3}$ was significantly larger during deflation than during inflation ($P < 0.001$). The percentage of *D* changed more linearly with the percentage of $V^{1/3}$ for large airways than for smaller airways, and the differences between inflation and deflation were not statistically significant. For smaller airways, the percentage of *D* changed dramatically at specific $V^{1/3}$, and the percentage of *D* also changed linearly with that of $V^{1/3}$. These results indicate that all airways behaved very similarly and isotropically, except at specific lung volumes.

Figure 10 shows the progressive average δ_D in larger (>300-μm-diameter) airways compared with smaller (<300-μm-di-

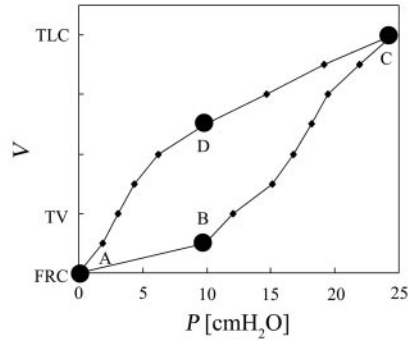

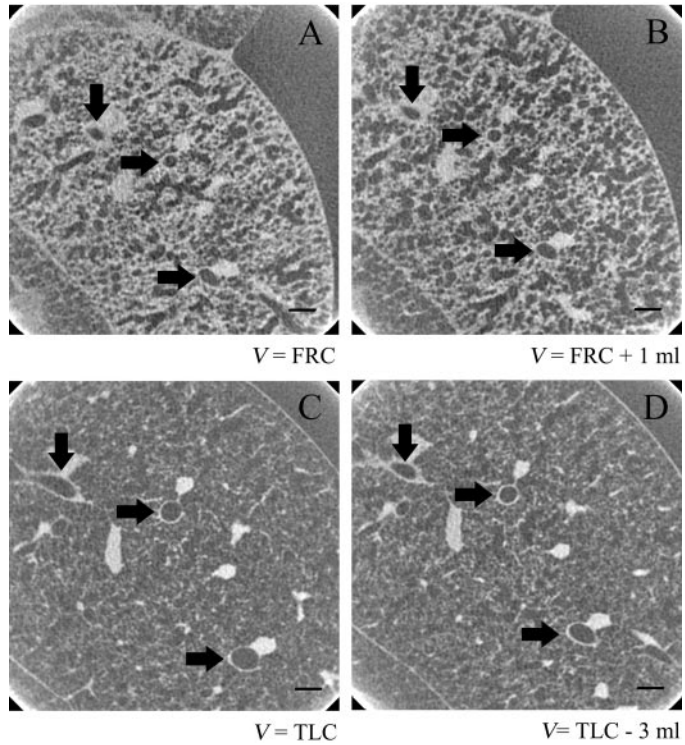

Fig. 5. Representative hysteresis of small airways against lung pressure. *Top*: pressure-volume (P-V) curve. *Bottom*: micro-CT images at V = FRC (*A*), V = FRC + 1 ml (inflation; *B*), V = FRC + 8 ml (TLC; *C*), and V = TLC − 3 ml (deflation; *D*). Same-direction arrows indicate the same airways. Lung pressure in *B* was approximately the same as that in *D*. TV, FRC + 2 ml (tidal volume ~7 ml/kg); TLC, FRC + 8 ml. Pressure at TLC was 26.52 ± 2.25 cmH_2O. Scale bars, 500 μm.

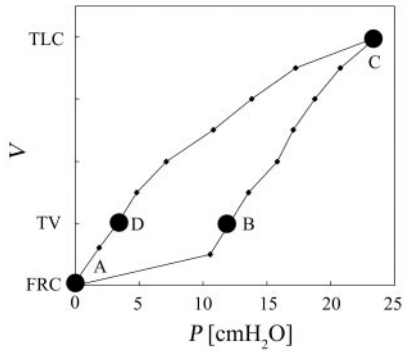

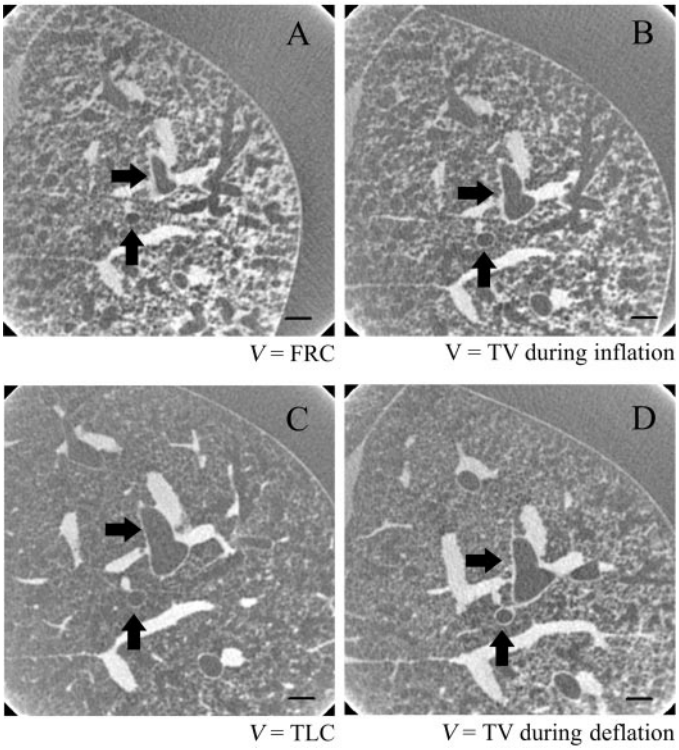

Fig. 6. Representative hysteresis of small airways against lung volume. *Top*: P-V curve. *Bottom*: micro-CT images at V = FRC (*A*), V = TV (inflation; *B*), V = FRC + 8 ml (TLC; *C*), and V = TV (deflation; *D*). TV, FRC + 2 ml (tidal volume ~7 ml/kg). Same-direction arrows indicate the same airways. Scale bars, 500 μm.

ameter) airways during inflation and deflation as a function of pressure. The localized pressure-δ_D curves differed between the smaller and larger airways; for smaller airways, *D* increased 36% at TV and 89% at TLC, whereas for larger airways, *D* increased 18% at TV and 47% at TLC. The hysteresis for larger airways was fairly moderate, whereas that for smaller airways was more pronounced. For 12 and 16 cmH_2O pressure, δ_D values for smaller airways were significantly larger during deflation than during inflation ($P < 0.001$), whereas δ_D for larger airways was statistically not so. During inflation, small airway *D* increased dramatically at a specific pressure; during inflation, δ_D for smaller airways was significantly larger at 20 than at 16 cmH_2O pressure ($P < 0.001$). This tendency is similar to that previously reported by Naureckas et al. (17). With further increase in pressure, *D* in small airways remained relatively constant. During deflation, *D* in small airways gradually decreased as pressure fell from 20 to 12 cmH_2O and then decreased dramatically when pressure reached 12 cmH_2O.

Bronchial length. Figure 11 shows the average δ_L at TV and TLC during inflation as a function of *Z*. Although δ_L increased at lower *Z* as *Z* increased (*Z* = 8–11), it remained relatively constant at higher *Z* (*Z* = 12–16) at TV and TLC. δ_L was statistically larger at TLC than at TV at *Z* = 11–16 ($P < 0.05$). This difference was similar to that of δ_D shown in Fig. 7, although δ_L was smaller than δ_D in smaller airways (cf. Figs. 7 and 11).

Figure 12 shows the average length behavior for smaller (<300-μm-diameter) airways during inflation and deflation: the percentage of the average *L* as a function of the percentage of $V^{1/3}$ and the progressive average δ_L as a function of pressure. The percentage of *L* changed linearly with the percentage of $V^{1/3}$, and the differences between inflation and deflation were not statistically significant. These results indicate that *L* changed isotropically. *L* increased by 18% at TV and by 43% at TLC. δ_L was not statistically larger during deflation than during inflation, and it changed linearly with pressure during inflation and deflation, resulting in the absence of hysteresis.

Bronchial volume. Figure 13 shows the average airway volume (V_{aw}) for smaller (<300-μm-diameter) and larger (>300-μm-diameter) airways during inflation and deflation as a function of lung volume. The airway volume was calculated as follows: $V_{aw} = D^2 * L * \pi/4$. The values of airway and lung volume are presented as a percentage of the values at TLC. We found that the airway volume behaved more linearly with lung volume for larger airways than for smaller airways and that differences between inflation and deflation were not statistically significant. For the smaller airways, at lower and intermediate lung volume, airway volume was significantly larger during deflation than during inflation ($P < 0.001$). During inflation, airway volume was smaller at lower lung volume and larger at high lung volume. During deflation, airway volume was larger at high and intermediate lung volume and smaller at lower lung volume. Similar to the behavior of *D* as a function of $V^{1/3}$ (Fig. 9), airway volume behaved linearly with lung volume, except a specific lung volume.

Localized compliance. The localized compliances (C_{TV} and C_{TLC}) of individual airway segments were determined by using *Eq. 1*. Figure 14 shows the average C_{TV} and C_{TLC} as a function

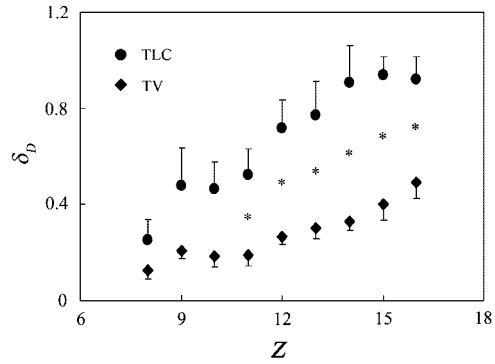

Fig. 7. Rate of diameter increase (δ_D, mean ± SE) at TV and TLC as a function of *Z*. Average diameter at *Z* = 8 (D_8) was 432 μm and that at *Z* = 16 (D_{16}) was 178 μm (21). *$P < 0.05$.

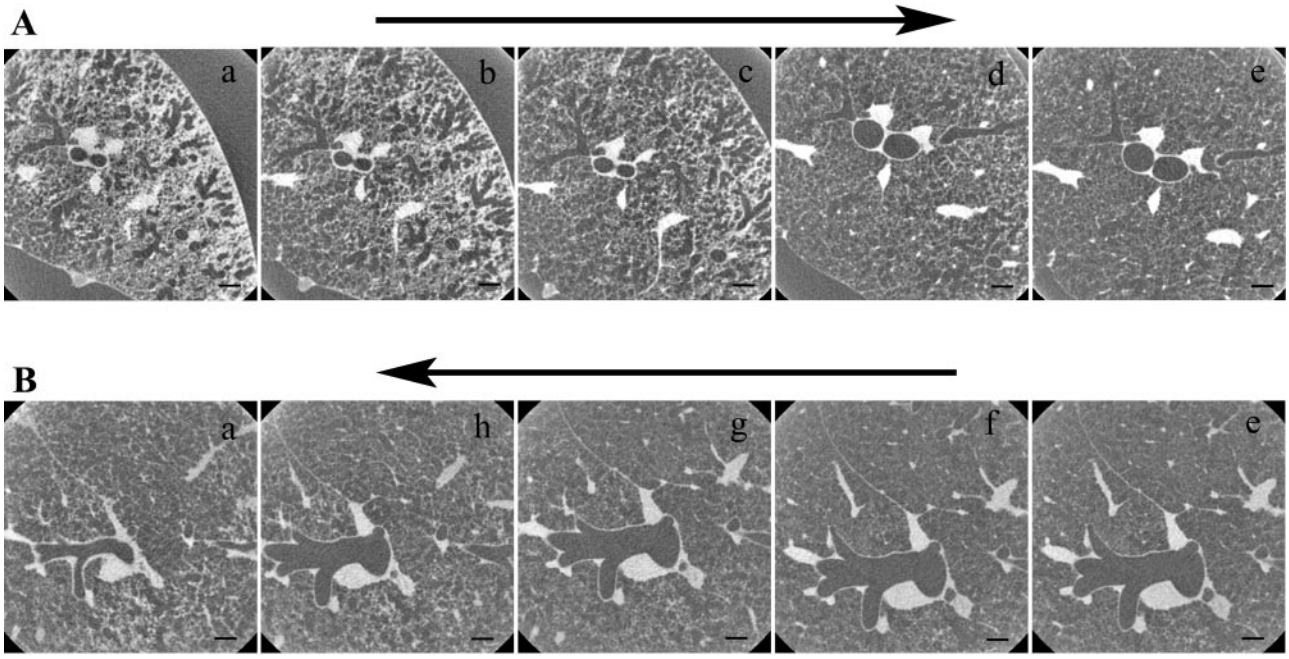

Fig. 8. Representative micro-CT images of the same airways during inflation (*A*) and deflation (*B*) at V = FRC (*a*), V = FRC + 2 ml (*b*), V = FRC + 4 ml (*c*), V = FRC + 6 ml (*d*), V = TLC (*e*), V = TLC − 2 ml (*f*), V = TLC − 4 ml (*g*), and V = TLC − 6 ml (*h*). Scale bar, 500 μm.

of *Z*. C_{TV} and C_{TLC} gradually increased with increasing *Z*, and C_{TLC} was significantly larger than C_{TV} at $Z = 12$–15 ($P < 0.05$). We calculated the average overall C_{TV} ($C_{\overline{TV}}$) and C_{TLC} ($C_{\overline{TLC}}$) as follows

$$C_{\overline{TV}} = \frac{TV - FRC}{(P_{TV} - P_{FRC})\cdot FRC}$$

$$C_{\overline{TLC}} = \frac{TLC - FRC}{(P_{TLC} - P_{FRC})\cdot FRC}$$

$C_{\overline{TV}}$ was 0.06 ± 0.004 and $C_{\overline{TLC}}$ was 0.10 ± 0.01, and C_{TV} and C_{TLC} above $Z = 9$ were significantly larger than $C_{\overline{TV}}$ and $C_{\overline{TLC}}$ (Fig. 14; $P < 0.05$).

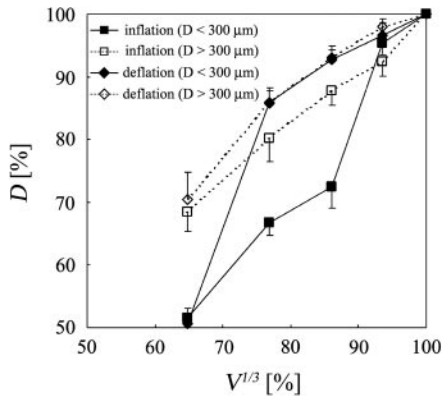

Fig. 9. Percentage of diameter (*D*) as a function of percentage of $V^{1/3}$ during inflation and deflation. Values are means ± SE. $P < 0.001$ for differences of smaller airways between inflation and deflation at TV and TV + 2 ml and for difference of smaller airways between TV + 2 ml and TV + 4 ml during inflation.

DISCUSSION

For analyzing lung mechanics, the SCT imaging method proposed by Sera et al. (21) is more appropriate than conventional imaging using metal dust. The diameter of the small airways analyzed in the present study was as small as 150 μm. On the basis of previous results (5, 20, 29), diatrizoate solution probably permeates lung tissue by pinocytosis and through the disturbed tight junctions, and this solution does not fix the lung tissue. We confirmed previously that no leakage of the radiopaque solution occurred into the alveolar air spaces, that alveoli were not collapsed, and that the SCT method could clearly identify airway geometry by comparison with the tantalum dust insufflation.

The localized mechanical properties of small airways are highly affected by surrounding lung parenchyma (Fig. 1). In

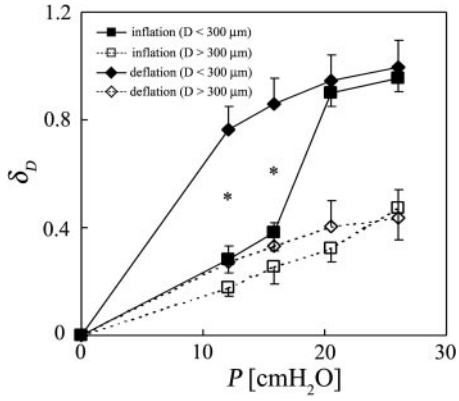

Fig. 10. Diameter increase (δ_D, mean ± SE) as a function of lung pressure (P) during inflation and deflation. *$P < 0.001$ for differences of smaller airways between inflation and deflation at 12 and 16 cmH_2O and for difference of smaller airways between 16 and 20 cmH_2O during inflation.

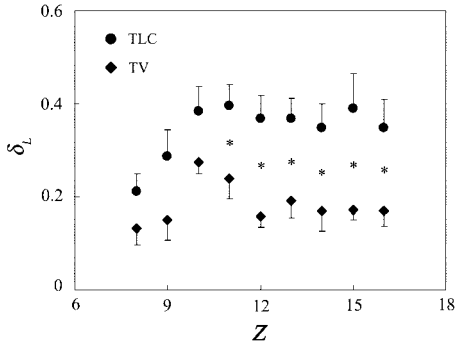

Fig. 11. Length increase (δ_L, mean ± SE) at TV and TLC as a function of *Z*. Average length was 853 μm at $Z = 8$ (L_8) and 452 μm at $Z = 16$ (L_{16}) (21). *$P < 0.05$.

our study, the localized airway compliance was defined as the compliance normalized by the airway segment volume at FRC and was similar to normalized lung macroscopic compliance by lung volume at FRC [specific compliance defined as $\Delta V/(\Delta P * FRC)$]. Tiddens et al. (27) calculated the specific compliance of isolated human small (1.3 ± 0.39 mm average diameter) airway segments on the basis of the volume of the segments inflated from 0 to 15 cmH_2O in Krebs buffer and reported that the average specific compliance was 0.053. Our results show a smaller compliance: C_{TV} at $Z = 8$ was 0.043 for $D \sim 430$ μm (21). This difference in compliance indicates that the localized compliance is indeed influenced by the surrounding lung parenchyma and surface tension and that isolated

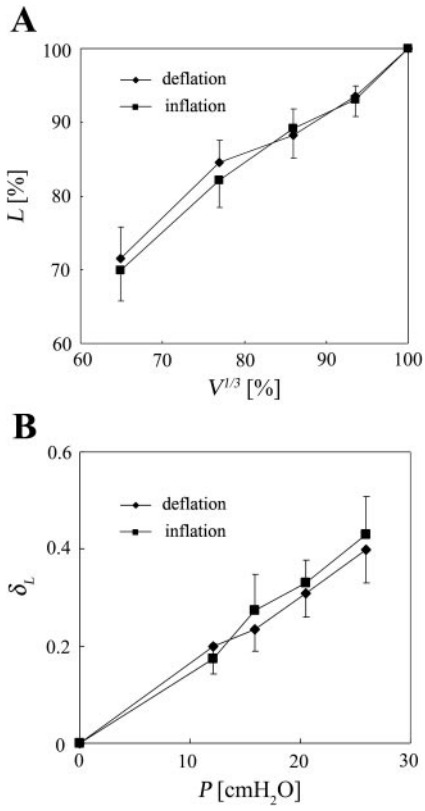

Fig. 12. Length behavior (mean ± SE) for smaller (<300-μm-diameter) airways during inflation and deflation. *A*: percentage of length as a function of percentage of $V^{1/3}$. *B*: δ_L as a function of pressure.

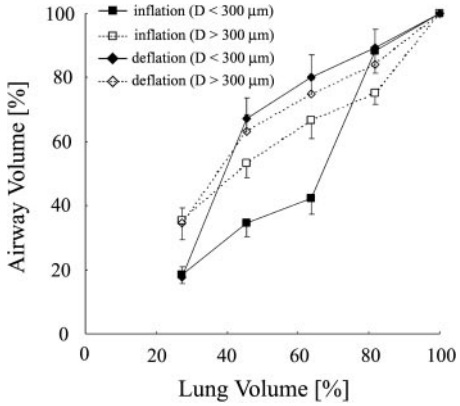

Fig. 13. Percentage of airway volume as a function of percentage of lung volume during inflation and deflation. $P < 0.001$ for differences of smaller airways between inflation and deflation at 45% and 63% of lung volume and for difference of smaller airways between 63% and 80% of lung volume during inflation.

airways are more compliant than intact airways (8, 9, 25). Although compliance is partially influenced by surface tension, in the experiments by Tiddens et al. (27) the isolated airway segments were placed in an organ bath and filled with buffer, and thus the effects of surface tension were eliminated. It is well known that a saline-filled lung, which does not exhibit air-surfactant interface or surface tension, is more compliant than a normal lung. Furthermore, small airways in lung parenchyma are surrounded by many alveoli (Fig. 1). The alveolar wall acts as a spring, and the localized compliance is determined not only by airway pressure but also by interdependence between the airway and the alveoli (3, 15), and therefore isolated airways are more compliant.

The small airways in our study exhibited hysteresis; *D* was larger during deflation than during inflation at 12 and 16 cmH_2O pressure ($P < 0.001$; Fig. 10), although *L* remained relatively constant (Fig. 12). Because the larger airways are inherently stiffer than smaller airways, diameter of the smaller airways is more affected by changes in lung volume of the tissue surrounding them, whereas larger airways are relatively unaffected. Smooth muscle tone and surface tension are important factors in hysteresis (19). Using a tantalum bronchogram technique, Hughes et al. (8) analyzed the change in

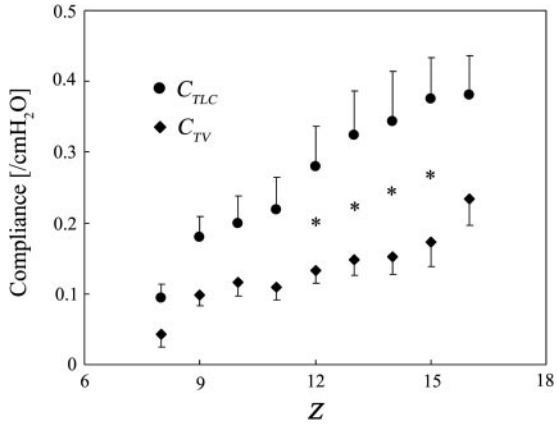

Fig. 14. Localized compliance at TV (C_{TV}) and TLC (C_{TLC}) as a function of *Z*. Values are means ± SE. *$P < 0.05$.

bronchial *L* and *D* of excised dog lungs during inflation and deflation. They reported that the bronchial segments did not exhibit hysteresis in *L* or *D* and explained that the reason was that the surfactant did not completely cover the entire surface of the large bronchi ($D = 0.1–1.17$ cm). The airway behavior in large airways is hardly affected by airway surfactant and, so, exhibits less hysteresis. A saline-filled lung without lung surfactant does not exhibit hysteresis in its P-V curve. Tiddens et al. (27) reported that isolated human small airways ($D = 1.3 \pm 0.39$ mm) exhibited hysteresis in the P-V curve. In their experiments, the airway segments were placed in an organ bath and filled with buffer, and the observed hysteresis in the P-V curve was caused by the behavior of *D*. Shardonofsky et al. (22) lengthened and shortened dog bronchial segments ($Z = 4$ or 5) in the axial direction in Krebs solution and reported no significant differences in axial strain between the lengthened and shortened airways and reported no hysteresis. Our results are consistent with all these previous results. However, although Tiddens et al. reported that *D* gradually increased as pressure increased, we found that *D* changed dramatically at a specific pressure (Fig. 10).

This dramatic change in *D* at a specific pressure can be explained as follows. As shown in Fig. 10, *D* sharply changed at 16 cmH_2O pressure during inflation and at 12 cmH_2O pressure during deflation. This variation in *D* could be closely associated with the airway opening-and-closing process. Using a model, Gaver et al. (4) studied the airway opening process in experiments and reported that pressure at which *D* sharply increased depended on *D* and surface tension. Using the tantalum bronchograms obtained by microfocal X-ray imaging, Naureckas et al. (17) analyzed *D* of excised rat lungs during inflation and reported that *D* increased from 400 to 700 μm when the lung pressure was increased slowly from 0 to 25 cmH_2O. Our results showed similar trends (Fig. 10), in that *D* gradually increased when pressure was increased from 0 to 12 cmH_2O, and then the airways appeared to "pop" open when pressure was further increased. The opening process of small airways during inflation is determined by tissue elasticity and surface tension. At low pressure before the airways suddenly opened, a balance among tissue elasticity, surface tension, and transmural pressure was maintained, and thus *D* was relatively constant (Fig. 10). At a specific pressure, the balance was not maintained, and thus *D* dramatically increased (Fig. 10).

All airways did not deform in the same way: the smaller airways expanded and contracted more at lower pressure than did the larger airways. In our study, early in the inflation, the air space increased, but *D* of small airways remained relatively constant, whereas late in the inflation, the air space increased only slightly but *D* dramatically increased (Fig. 8*A*). A key result in our study is that small airways were more compliant at higher *Z* (Fig. 14). Martin and Proctor (14) measured the P-V curve of dog bronchi and reported that peripheral airways were more compliant than central airways. Naureckas et al. (17) reported that the specific pressure at which *D* dramatically increased depended on *D* and that pressure was lower in smaller airways. Mercer et al. (16) analyzed alveolar diameter of fixed rat lungs at various lung pressures and reported that the diameter increased remarkably between 0 and 10 cmH_2O (between 43.3 ± 2.3 and 100.3 ± 3.3 μm) and was approximately constant at >10 cmH_2O. Their results indicate that the smaller airways opened at lower pressure during inflation than did larger airways. In addition, dC_{TV}/dZ increased and dC_{TLC}/dZ decreased with increasing *Z* at higher *Z* (Fig. 14).

Interestingly, *D*, especially of smaller (<300-μm-diameter) airways, did not change linearly with $V^{1/3}$, although as would be expected, *L* did (Figs. 9 and 12*A*). Our results differ from those of Hughes et al. (8), who reported that there were no differences in *D* and *L* between large and small bronchi and that *D* and *L* changed linearly as $V^{1/3}$. Furthermore, the airway volume of smaller airways (unlike the larger airways) did not behave linearly with lung volume (Fig. 13). Previous studies suggested that airway properties were homogeneous. However, the airway wall structure varies along the path. Ma et al. (13) analyzed the mechanical properties of muscle strips of canine airways of different generations (*Z*) and demonstrated the heterogeneity of airway smooth muscle, thus indicating that small and larger airways may not expand similarly.

We do not consider that the difference in larger and smaller airway behavior is due to the effects of the peribronchial sheath, present around the larger bronchi. Inasmuch as the ventilation-distension process is essentially static, the pressure within the sheath would be expected to reflect closely the surrounding alveoli.

In summary, the SCT method allowed successful visualization of small airways under near-physiological conditions: the airways were embedded in lung parenchyma without dehydration or fixation. Our study is the first to evaluate localized airway compliance by using this method, which may have physiological and clinical applications in animal experiments. Compared with the values of *D* and *L* at FRC, *D* was 36% higher at TV and 89% at TLC and *L* was 18% higher at TV and 43% at TLC. All airways did not deform in the same manner. Large airways demonstrated similar inflation and deflation diameter change patterns; however, with increasing *Z*, local compliance of the small airways exhibited clear hysteresis. During the earlier steps of inflation, small airways inflated similarly to the larger airways, following a path very dissimilar from their deflation path, but at above ~16 cmH_2O, the small airways experienced a rapid increase in diameter and thereafter followed a path very close to the deflation path at high lung volume.

REFERENCES

1. **Cassidy KJ, Bull JL, Glucksberg MR, Dawson CA, Haworth ST, Hirschl R, Gavriely N, and Grotberg JB.** A rat lung model of instilled liquid transport in the pulmonary airways. *J Appl Physiol* 90: 1955–1967, 2001.
2. **Comer JK, Kleinstreuer C, Hyun S, and Kim CS.** Aerosol transport and deposition in sequentially bifurcating airways. *J Biomech Eng* 122: 152–158, 2000.
3. **Elad D, Kamm RD, and Shapiro AH.** Tube law for the intrapulmonary airway. *J Appl Physiol* 65: 7–13, 1988.
4. **Gaver DP III, Samsel RW, and Solway J.** Effects of surface tension and viscosity on airway reopening. *J Appl Physiol* 69: 74–85, 1990.
5. **Haller C, Schick CS, Zorn M, and Kubler W.** Cytotoxicity of radiocontrast agents on polarized renal epithelial cell monolayers. *Cardiovasc Res* 33: 655–665, 1997.
7. **Heil M.** Airway closure: occluding liquid bridges in strongly buckled elastic tubes. *J Biomech Eng* 121: 487–483, 1999.
8. **Hughes JM, Hoppin FG Jr, and Mead J.** Effect of lung inflation on bronchial length and diameter in excised lungs. *J Appl Physiol* 32: 25–35, 1972.
9. **Hyatt RE and Flath RE.** Influence of lung parenchyma on pressure-diameter behavior of dog bronchi. *J Appl Physiol* 21: 1448–1452, 1966.

10. **Klingele TG and Staub NC.** Terminal bronchiole diameter changes with volume in isolated, air-filled lobes of cat lung. *J Appl Physiol* 30: 224–227, 1971.
11. **Lai YL and Hildebrandt J.** Respiratory mechanics in the anesthetized rat. *J Appl Physiol* 45: 255–260, 1978.
12. **Lamm WJ, Hildebrandt JR, Hildebrandt J, and Lai YL.** End-expiratory volume in the rat: effects of consciousness and body position. *J Appl Physiol* 53: 1071–1079, 1982.
13. **Ma X, Li W, and Stephens NL.** Heterogeneity of airway smooth muscle at tissue and cellular levels. *Can J Physiol Pharmacol* 75: 930–935, 1997.
14. **Martin HG and Proctor DF.** Pressure-volume measurements on dog bronchi. *J Appl Physiol* 13: 337–343, 1958.
15. **Menkes H, Gamsu G, Schroter R, and Macklem PT.** Interdependence of lung units in isolated dog lungs. *J Appl Physiol* 32: 675–680, 1972.
16. **Mercer RR, Laco JM, and Crapo JD.** Three-dimensional reconstruction of alveoli in the rat lung for pressure-volume relationships. *J Appl Physiol* 62: 1480–1487, 1987.
17. **Naureckas ET, Dawson CA, Gerber BS, Gaver DP III, Gerber HL, Linehan JH, Solway J, and Samsel RW.** Airway reopening pressure in isolated rat lungs. *J Appl Physiol* 76: 1372–1377, 1994.
18. **Okazawa M, Paré PD, and Lambert RK.** Compliance of peripheral airways deduced from morphometry. *J Appl Physiol* 89: 2373–2381, 2000.
19. **Sakai H and Hoppin FG Jr.** Hysteresis of contracted airway smooth muscle. *J Appl Physiol* 68: 1251–1261, 1979.
20. **Schick CS and Haller C.** Comparative cytotoxicity of ionic and non-ionic radiocontrast agents on MDCK cell monolayers in vitro. *Nephrol Dial Transplant* 14: 342–347, 1999.
21. **Sera T, Fujioka H, Hokota H, Makinouchi A, Himeno R, Schroter S, and Tanishita K.** Three-dimensional visualization and morphometry of small airways from microfocal X-ray computed tomography. *J Biomech* 36: 1587–1594, 2003.
22. **Shardonofsky FR, Officer TM, Boriek AM, and Rodarte JR.** Effects of smooth muscle activation on axial mechanical properties of excised canine bronchi. *J Appl Physiol* 90: 1258–1266, 2001.
23. **Sittipong R and Hyatt RE.** Static mechanical behavior of bronchi in excised dog lung. *J Appl Physiol* 37: 201–206, 1974.
24. **Takezawa J, Miller FJ, and O'Neil JJ.** Single-breath diffusing capacity and lung volumes in small laboratory mammals. *J Appl Physiol* 48: 1052–1059, 1980.
25. **Takishima T, Sasaki H, and Sasaki T.** Influence of lung parenchyma on collapsibility of dog bronchi. *J Appl Physiol* 38: 875–881, 1975.
26. **Tashkin DP.** The role of small airway inflammation in asthma. *Allergy Asthma Proc* 23: 233–242, 2002.
27. **Tiddens HA, Hofhuis W, Bogaard JM, Hop WC, de Bruin H, Willems LN, and de Jongste JC.** Compliance, hysteresis, and collapsibility of human small airways. *Am J Respir Crit Care Med* 160: 1110–1118, 1999.
28. **Toriwaki J and Mori K.** Distance transformation and skeletonization of 3D pictures and their applications to medical images. In: *Digital and Image Geometry*, edited by Bertrand G, Imiya A, and Klette R. Tokyo: Springer, 2001, p. 412–428.
29. **Waldron RL II, Bridenbaugh R, Purkerson M, and Dempsey EW.** The effect of angiographic contrast media at the cellular level in the brain. *Radiology* 108: 187–189, 1973.
30. **Weibel ER.** *Morphometry of the Human Lung*. New York: Academic, 1963, p. 136–143.
31. **Zhang YL, Matar OK, and Craster RV.** A theoretical study of chemical delivery within the lung using exogenous surfactant. *Med Eng Phys* 25: 115–132, 2003.